Res Mechanica **29** (1990) 197–219

A Dislocation Model for Creep in Engineering Materials

N. M. Ghoniem

Mechanical, Aerospace and Nuclear Engineering Department, University of California, Los Angeles, California 90024, USA

J. R. Matthews

Theoretical Physics Division, Harwell Laboratory, Oxfordshire OX11 0RA, UK

&

R. J. Amodeo

Xerad Inc., 1526 14th Street, Suite 102, Santa Monica, California 90404, USA

(Received 15 March 1989)

ABSTRACT

A simple dislocation model for creep in engineering materials has been constructed in order to predict high temperature deformation under arbitrary time-dependent stress and temperature histories. The model also has the advantage of being compatible with the rate theory of radiation damage, which allows radiation effects to be included. The basis of the model is the generation and immobilization of dislocations at subgrain boundaries, the recovery of the static dislocations at the boundaries, the dynamics of nucleation and growth of subgrains, and the evolution of the dislocation density in the boundaries. The effects of solutes and hardening precipitates are included. Example calculations are given for the martensitic steel, HT-9.

1 INTRODUCTION

The materials which are used in the construction of load-bearing components in the core of fission reactors and in the first wall of future fusion reactors are subjected to conditions where both thermal creep and radiation damage effects are significant. The rate theory has proved

Res Mechanica 0143-0084/90/$03·50

useful in understanding void swelling and anisotropic growth in metals subjected to displacement damage by fast neutrons.[1] This tool should also be useful in understanding creep in the irradiation environment, where some progress has already been made. The Nabarro model of dislocation climb creep[2] has been adapted to fit within the framework of the rate theory.[3] In this form, the model has been used to reproduce the thermal creep rates, stress sensitivities, and dislocation density for 316 stainless steel in the stress range of 10 to 100 MPa at 700 °C.[4] Irradiation creep by the stress-induced preferential absorption of point-defects model[5,6] may be calculated concurrently with thermal creep. Other point-defect sinks may be included in the rate equations permitting both the description of swelling and growth in the presence of an applied stress, and the effect of irradiation on thermal creep. The effects of irradiation-driven multiplication and recovery on thermal creep are implicit in the model.

In previous models, the omission of dislocation glide as a source of strain and dislocation multiplication is a major limitation on their applicability, particularly for higher stresses. In this paper we develop the framework of a dislocation model of thermal creep using the rate theory, including the effects of radiation damage. In order to simplify this task and apply the model to engineering materials, only one representative dislocation system is treated, rather than the three orthogonal systems in the climb creep theory.[3]

The model described here is intended to be used in the study of the behavior of engineering materials rather than pure metals or simple alloys. For this reason the components of the model governing various dislocation interactions are deliberately left simple. Many steels exhibit the formation of dislocation cells or subgrain boundaries during high temperature deformation. One of the key aspects of this work is the inclusion of subgrain boundary behavior. The present model is closely related to the work of Nabarro, Bullough, and Matthews on the effects of irradiation on creep[7] in the sense that many of the reactions controlling creep take place within or adjacent to the subgrain walls. It also generalizes the mechanical equation-of-state approach pioneered by Gittus.[8,9]

The subgrains also limit dislocation movement and the subgrain diameter is a key parameter in determining the creep rate under many conditions.[10] The range of processes involved have recently been reviewed,[11] particularly Holt's hypothesis[12] that subgrains nucleate from fluctuations in the local dislocation distribution. Detailed computations with the newly developed dislocation dynamics technique[13] show that the emergence of an organized subgrain structure results as a conse-

quence of elastic energy minimization. The onset of nucleation, however, is dictated by nonlinear dislocation reactions. This provides a basis for including a treatment of subgrain dynamics in the model.

The choice of a simple dislocation model has many advantages over phenomenological models and equations of state with variables not identified with microstructural features. Dislocation models, even as simple as those presented here, permit realistic deformation rates to be estimated without empirical fitting. Although some free parameters have to be included for engineering materials (which are complex in composition and microstructure), the main features of the behavior are inherent in the structure of the model.

2 OUTLINE OF THE DISLOCATION MODEL

A number of characteristics have been identified with the dislocation structure in metals during high temperature deformation (see Ref. 14 or 15 for discussion). These are:

(1) Dislocation pileups and the debris associated with cold work are not observed;
(2) The dislocations form a polygonal network, which is seen to nucleate subgrain boundaries if the temperature is high enough and the stresses low enough for climb into the boundaries to keep pace with dislocation generation;
(3) The network and subgrain dimensions are inversely proportional to the applied stress;
(4) The dislocation density within the network cells or subgrains is low and increases with the square of the applied stress;
(5) The misorientation across sub-boundary walls is subject to a long transient only saturating after tens of percent strain, but the value is insensitive to applied stress and temperature.

This behavior is widely seen in metals and alloys. The formation of sub-boundaries may be delayed to higher temperatures in materials with low stacking fault energy. Sub-boundaries may also be inhibited in dispersion-hardened alloys and alloys where solute hardening limits dislocation motion. Despite this, subgrains are commonly seen in steels where the stacking fault energy is low, there is extensive precipitation, and there are substantial concentrations of hardening solutes.[16–18]

The essential features, described in detail below, are dislocation reactions which take place either within the subgrains or at the subgrain boundary. The boundary consists of sub-boundary dislocations, which

have formed low energy configurations and have neutralized their long-range elastic fields, and static dislocations which form dipoles or multipolar bundles with the sub-boundary dislocations. The interactions between these two types of dislocations are crucial to the operation of the model. The physical processes considered are:

(1) Multiplication of dislocations by interaction between the mobile dislocations within the subgrains;
(2) Annihilation of dislocations by mutual interaction of mobile dislocations within the subgrains;
(3) Annihilation of dislocations within the sub-boundary wall;
(4) Absorption of dislocations in the wall;
(5) Emission of dislocations from the wall;
(6) Nucleation of new subgrains from dislocations within the cells;
(7) Growth of the subgrains by coalescence driven by the sub-boundary energy.

All of these processes, including the newer reactions involving the sub-boundaries, have been discussed by others[8,19–21] but we believe that this is the first attempt to form them into a comprehensive creep model.

2.1 Dislocation multiplication and immobilization

A convenient starting point in our model is the Orowan equation which expresses the macroscopic creep strain rates, $\dot{\varepsilon}$, as the aggregate strain rate produced by the glide of mobile dislocations. This is given by

$$\dot{\varepsilon} = b\rho_m v_g \tag{1}$$

where v_g is the dislocation glide velocity, b is the Burgers vector magnitude, and ρ_m is the mobile dislocation density. It is assumed that the glide process is easy and that climb driven by the applied stress does not contribute to the macroscopic strain.

New mobile dislocations are generated from sources operating by the interaction between existing mobile dislocations or from favorable sites on the sub-boundaries. Once formed, they move an average distance before being immobilized. This distance is assumed to be the subgrain diameter, $2R_{sb}$, unless some other obstacle (e.g. large impenetrable precipitates, platelets, or the grain boundaries) has smaller separations.

For the moment we will ignore recovery processes. The density of sources from interactions within the mobile dislocation population is approximately ρ_m; on average they operate with a frequency $v_g\rho_m^{1/2}$, and produce a line length ρ_m each time. The mobile dislocation population

then builds up at a rate

$$\dot{\rho}_m = \rho_m^{3/2} v_g \tag{2}$$

The inclusion of immobilization terms is not appropriate at this stage and, where multiplication is dominated by reactions within the mobile population, other processes governing recovery take place. This is particularly true during initial loading at low temperatures where subgrains do not form, and during saturation for very high dislocation densities.

Once subgrains have formed, the walls not only act as barriers for the mobile dislocations but also provide sources. The density of links that have the potential of action as dislocation sources is $\frac{1}{2}h^2 R_{sb}$ where h is the dislocation spacing within the wall and R_{sb} is the subgrain radius. The spacing is related to the density of static dislocations, ρ_s, and that of the boundary dislocations, ρ_b, by

$$h = 1/(\rho_s + \rho_b) R_{sb} \tag{3}$$

Interaction between dislocations immobilized at the sub-boundary and the sub-boundary dislocations disturbs the local structure and permits some dislocation segments within the boundary to become active. We assume that the fraction of links that operate is proportional to ρ_s/ρ_b (i.e. the ratio of the relative spacing at the boundary of dislocations which are not in low energy configuration, to the spacing of the boundary dislocations). The frequency of operation of the source is of the order v_g/h but the line length generated is $2R_{sb}$. We can now construct a pair of rate equations for the mobile and static dislocation populations:

$$\dot{\rho}_m = \beta \rho_s R_{sb} v_g / h^2 - \rho_m v_g / 2R_{sb} \tag{4}$$

$$\dot{\rho}_s = \rho_m v_g / 2R_{sb} \tag{5}$$

where β is a factor controlling the density of sources and is treated as a fitting variable in the model.

2.2 Internal stress

Internal stresses are caused by opposition to dislocation motion and there are three processes of quite different character responsible for their existence. The first source arises from precipitates and other dislocations which oppose dislocation motion. If the effective obstacle spacing is λ, the internal stress that must be overcome by a dislocation or bowing out between obstacles is $\mu b/2\pi\lambda$, where μ is the shear modulus. If both precipitates and dislocation obstacles are present, the

spacing is given by

$$\lambda = 1/(1/\lambda_d + 1/\lambda_p) \tag{6}$$

where $\lambda_d = 1/\rho_m^{1/2}$ and $\lambda_p = 1/(N_p r_p)^{1/2}$. λ_d is the inter-dislocation spacing, λ_p is the inter-precipitate spacing, N_p is the volume concentration of precipitates, and r_p is the mean radius.

The second source of internal stress is the cumulative effect of the fields of dislocations that have not neutralized their long-range elastic fields by moving into low energy configurations. The sum of the contribution of these dislocations forms a fluctuating field. The mobile dislocations will be accelerated through regions where the field is attractive but held up where the field is repulsive. The sub-boundary dislocations themselves do not contribute to the internal stress at distances from the boundary much greater than the spacing of the dislocations within the boundary.[22] The main effect arises from the static dislocations at the boundary with a contribution to the internal stress of $\xi\mu b\rho_s^{1/2}$, where ξ is a constant of the order of unity. Combining these effects we define the long-range internal stress σ_i as

$$\sigma_i = \mu b/2\pi\lambda + \xi\mu b\rho_s^{1/2} \tag{7}$$

The third process which opposes dislocation motion is due to the frictional resistance to glide. In engineering alloys this results almost entirely from oversize solutes which are added to increase the strength of the material. The solutes control the dislocation velocity at low stresses, but if the applied stress is high enough for the dislocation to break away from solute clouds or solute pinning there will still be a friction force opposing glide. The theory of solute hardening is complex[23] and engineering alloys are generally both concentrated and dilute alloys with many elements. Some of these elements may be oversize, undersize, substitutional, or interstitial. For this study we will represent this effect by just a single stress, σ_0, which is characteristic of the alloy being considered. In well-annealed materials, without hardening precipitates and heat treatment to remove precipitates, σ_0 can be identified with the initial flow stress. These considerations lead to an effective stress on the dislocation, σ_e, given by

$$\sigma_e = \sigma_a - \sigma_i - \sigma_0 \tag{8}$$

where σ_a is the applied stress.

2.3 Dislocation velocity

In the model described here, the dislocation velocity does not, in practice, greatly influence the steady-state creep rate over much of the

range of interest. Dislocation glide is sufficiently easy for recovery processes to be rate-limiting. However, the form of the velocity dependence on stress controls the relationship between dislocation density and stress and hence, indirectly, the strain rate. The glide velocity is also important in determining short-term transients, although there are also longer-term transients determined by the sub-boundary behavior.

For low applied stresses where the effective stress felt by the dislocation is below the friction stress for glide, dislocation motion is viscous in nature. In pure metals and simple concentrated alloys, the glide velocity will be determined by the nucleation and diffusion of kinks and jogs. In most engineering alloys, solute effects dominate.

Solutes can affect dislocation motion in a number of ways. For low stresses, a dilute solute can form a Cottrell atmosphere which then produces a drag force resisting motion. This presupposes that dislocations do not form a sink for the solute. In this case, the dislocation velocity is given by[24,25]

$$v_g = D_a kTb\sigma_e/[c_0(\beta^*)^2 \ln (R/r)] \tag{9}$$

where σ_e is the effective stress, c_0 is the uniform volume concentration of the solute, D_a is the solute diffusion coefficient, R is the outer cutoff radius which may be assumed to be $\rho_m^{-1/2}$, and r is the inner cutoff radius given by the greater of β^*/kT and the core radius of the dislocation. The quantity β^* is given by[26]

$$\beta^* = (\mu b/3\pi)[(1+\nu)/(1-\nu)](v_s - v_a) \tag{10}$$

where ν is Poisson's ratio, v_s is the solute atomic volume, and v_a is the matrix atomic volume. As the dislocation velocity increases, the solute has difficulty keeping up with the dislocation; and when the stress on the dislocation exceeds around $17c_0\beta^*/b$, the dislocation breaks free. The residual friction stress is of the order $\pi c_0\beta^*/b$.[26]

The other main effect of solutes arises when solute atoms are trapped at the dislocation core, which is usually a precursor to precipitate formation. In this case, the velocity is given by[26]

$$v_g \approx 2bv_d \exp(-W_a/kT) \sinh(\sigma_e b^2 l_a/kT) \tag{11}$$

where v_d is the dislocation vibrational frequency, W_a is the activation free energy for core diffusion of the solute, and l_a is the spacing of the solute atoms in the core. Dislocation breakaway from the core solute atoms can only occur for stresses on the dislocation exceeding around $\mu\delta_a/l_a$ (δ_a being the misfit parameter), which for saturated cores is very large. As in the case of frictional effects on dislocations, the complex

makeup of engineering alloys makes it difficult to construct a comprehensive treatment of dislocation viscous motion. For the present model, an empirical glide velocity is used of the form

$$v_g = a_1 \exp(-W_g/kT)\sigma_e\Omega/kT \tag{12}$$

where a_1 and W_g are parameters to be fitted in the model and Ω is the atomic volume.

The other possibility for the limiting process for dislocation glide is the cutting of obstacles. This may be either the intersection of dislocations forming jogs or the cutting of coherent or semi-coherent precipitates. The general form of this process used in the model is

$$v_g = \nu_d \lambda \sinh(\sigma_e b^2 \lambda/2kT) \exp(-U_g/kT) \tag{13}$$

where U_g is the activation energy for the process, which is approximately twice the jog formation energy for dislocation intersection.

2.4 Climb and recovery

Climb in the non-irradiation environment involves both the emission and absorption of vacancies, except for very limited transients or extreme conditions where a rapidly climbing dislocation leaves a supersaturation of vacancies or interstitials. For less extreme cases, it is necessary to consider the sources and sinks of the vacancies involved in climb (the path of the vacancies), and whether there are limitations on the absorption of vacancies by the dislocations. In the irradiation environment, the effect of vacancies and interstitials produced by displacement damage must also be taken into account.

Climb recovery, for both mobile and static dislocations, can be considered as the climbing together of dislocation dipoles. For simplicity we will treat the climbing of a dislocation into a sub-boundary wall without annihilation by the same process. The dislocations in a dipole exert a mutual stress which favors climb:

$$\sigma_c = \mu b/2\pi(1-\nu)s \tag{14}$$

where s is the separation of the dislocations in the dipole. If the thermal equilibrium concentration of vacancies is c_v^e, the local vacancy concentration close to individual dislocations will be enhanced or reduced, depending on the nature of the interaction:

$$c_{vd}^e = c_v^e \exp\left(\pm\frac{\sigma_c\Omega}{kT}\right) \simeq c_v^e\left(1 \pm \frac{\sigma_c\Omega}{kT}\right) \tag{15}$$

where the subscript d refers to dislocations in dipole configuration.

With no loss of generality, we will only consider dipoles where the vacancy concentration is enhanced.

The rate-theory formulation will now be used to make the inclusion of irradiation effects in the model easier. The net flow of vacancies into dislocations is given by:

$$\frac{dq_d}{dt} = k_{id}^2 D_i c_i - k_{vd}^2 D_v c_v + k_{vd}^2 D_v c_{vd}^e \tag{16}$$

where k_{id}^2, D_i, and c_i are respectively the dislocation sink strength for interstitials, the interstitial diffusion coefficient, and the interstitial bulk concentration, with similar terms for vacancies subscript v. Under irradiation, the balance of interstitial and vacancy concentration is controlled by the rate equations[1]

$$\frac{\partial c_i}{\partial t} = K + k_i^2 D_i c_i - \alpha c_i c_v \tag{17}$$

$$\frac{\partial c_v}{\partial t} = K + K_v^e + k_v^2 D_v c_v - \alpha c_i c_v \tag{18}$$

where K is the rate of production of Frenkel pairs, k_i^2 and k_v^2 are the sum of the sink strength from all the potential sinks for interstitials and vacancies, K_v^e is the sum of the vacancy emission rates for all the sinks, and α is the rate constant governing recombinations of interstitials and vacancies. In addition to eqns (17) and (18), there will be an equation similar to eqn (16) for each type of sink.

The most important problem associated with this formulation is the derivation of the sink strength of the dislocations. The most reliable treatment of the sink strength, taking into account the effect of the elastic interaction between the dislocation and the point defects, is that of Rauh and Bullough.[27] Taking an approximation which is valid for the range of conditions of interest we have for network dislocations:

$$k_{\alpha N}^2 = -\frac{\pi \rho_N}{\ln\left[\left(\frac{1}{2}\right) e^{\gamma} (k_\alpha L_\alpha)\right]^{1/2}} \simeq -\frac{2\pi \rho_N}{\ln (k_\alpha L_\alpha)} \tag{19}$$

where the subscript α refers to either interstitials or vacancies, the subscript N refers to network dislocations, and γ is Euler's constant, ~0·5772. The parameter L_α is a length governing the range of the elastic interaction between the dislocation and the defects:

$$L_\alpha = (1 + \nu)\mu b \, |\Delta V_\alpha| / 3\pi(1 - \nu) kT \tag{20}$$

where ΔV_α is the relaxation volume of the defect. Typical values for these volumes are $\Delta V_v = -0{\cdot}5\,\Omega$ and $\Delta V_i = 1{\cdot}2\,\Omega$. The difference in L_α

between vacancies and interstitials is thought to give rise to the dislocation bias for interstitials which drives fast neutron-induced swelling. If the dislocation network is the only sink for vacancies, then $k_\alpha^2 = k_{\alpha N}^2$ and since $\ln(k_\alpha L_\alpha)$ is in the range -2 to -12, the sink strength of the mobile dislocations may be approximated by

$$k_{\alpha N}^2 = -2\pi\rho_N / \ln(\rho_N^{1/2} L_\alpha) \tag{21}$$

The sink strength for dislocations described above considers dislocations to be perfect sinks for defects and makes no allowance for rate limitation of the transfer of defects to jogs. Two considerations have to be taken into account. The first is that dislocations as a whole act as the sink for defects and not the individual jogs.[26,28] If the mean free path of the defect along the dislocation by pipe diffusion before it leaves the dislocation is greater than the mean spacing of jogs, then the whole dislocation acts as the sink. In simple terms, this condition is satisfied if $2U_j + Q_{\alpha c} - W_{\alpha c} < Q_\alpha$ where U_j is the jog formation energy, $Q_{\alpha c}$ is the activation energy for core diffusion of the defect, $W_{\alpha c}$ is the binding energy of the defect to the dislocation, and Q_α is the activation energy for lattice diffusion of the defect. Jog energies from elastic calculations are of the order $\mu\Omega/15$, which is small compared to diffusion activation energies. The binding energy of defects to dislocations is likely to be substantial, particularly for interstitials. For vacancies, where both emission and absorption are possible, the activation energy for core self-diffusion is $Q_p = E_v - W_{vc} + Q_{vc}$ where E_v is the vacancy formation energy. The activation energy for lattice self-diffusion is $Q_L = E_v + Q_v$. Substituting Q_p and Q_L in the inequality we get $2U_j + Q_p < Q_L$. Typical Q_p values are in the range 0·5 to 0·7 Q_L, and U_j is approximately 0·1 Q_L so the inequality is satisfied and we may safely assume that the dislocation and not the jogs are the sinks.

The transfer of defects into jogs on the dislocation is controlled by the transfer parameter[29,30]

$$\eta_\alpha = c_j b (a_{\alpha c} \nu_{\alpha c} / a_\alpha \nu_\alpha) \exp(-\Delta W_\alpha / kT) \tag{22}$$

where c_j is the jog concentration, $a_{\alpha c}$ and a_α are the geometric factors for correlating jumps in the core and in the lattice, $\nu_{\alpha c}$ and ν_α are the attempt frequencies for jumps in the core and in the lattice, and ΔW_α is the difference in activation energy for absorption onto the dislocation and for lattice migration. Recently, Argon and Moffatt have argued that extended dislocations have a frequency factor attenuated by a factor inversely proportional to the square of the separation of the partial dislocations, and hence are proportional to the square of the stacking fault energy.[31] This has been used to explain an apparent

dependence of creep rate on stacking fault energy in metals and alloys where climb recovery controls the creep rate.[32] The value of ΔW_α is not well known, but it is generally assumed to be negative,[1] though it could be positive with important implications on irradiation creep.[7] For the present we assume that ΔW_α is zero. Differences between the geometrical factors and frequencies for interstitials and vacancies have been proposed,[30] but a discussion of this is outside the scope of this paper and at present would have to be determined by fitting to observations. We will therefore use Argon and Moffatt's formulation[31] with an adjustable factor f_α which is unity for vacancies and can be set as desired for interstitials:

$$\eta_\alpha = 10^3 f_\alpha c_j b(\Gamma/\mu b)^2 \tag{23}$$

where Γ is the stacking fault energy. For austenitic steels, the stacking fault energy is low, and typically $0{\cdot}015\ \mathrm{J\,m^{-2}}$, $\eta \sim 10^{-3} c_j b$. For ferritic steels and aluminum alloys, the stacking fault energy is typically $0{\cdot}2\ \mathrm{J\,m^{-2}}$, $\eta \sim 0{\cdot}2 c_j b$. The thermal jog concentration is likely to be of the order of $10^{-3}/b$ at $\frac{1}{2}T_m$, but this may be enhanced by dislocation intersection processes or supersaturations of point defects. Taking the transfer rate into consideration, the sink strength becomes[28,31]

$$k^2_{\alpha N} = 2\pi\eta_\alpha \rho_N / [1 - \eta_\alpha \ln (\rho_N^{1/2} L_\alpha)] \tag{24}$$

For most conditions the sink strength is dominated by η_α.

We are, however, principally interested in the sink strength of dipoles. Provided the dipole separation is smaller than the scale of the surrounding dislocation structure, the dipole acts as a single sink for defects. Following the treatment of Hirth and Lothe,[26] but accounting for the effects of the elastic field and transfer rate limitation, the effective sink strength for each dislocation in the dipole becomes

$$k^2_{\alpha d} = 2\pi\eta_\alpha \rho_d / [1 - \eta_\alpha \ln (k^2_\alpha L_\alpha s)] \tag{25}$$

where s is the dipole separation distance.

Returning to the problem of climb recovery, we will assume that there is no radiation damage, hence $c_i = 0$ and $c_v = c_v^e$. The flow of vacancies to dislocations in eqn (16) becomes

$$\frac{\mathrm{d}q_d}{\mathrm{d}t} = k^2_{vd} D_s \sigma_c \Omega / kT \tag{26}$$

where the lattice self-diffusion coefficient $D_s = D_v c_v^e$. The climb velocity of the dislocations is given by

$$v_c = (\mathrm{d}q_d/\mathrm{d}t)/b\rho_d \tag{27}$$

Using eqns (14) and (25)–(27) and remembering that the rate of approach of the dislocations in the dipole is twice the individual sink rate, we obtain an expression for the rate of reduction of dipole separation:

$$ds/dt = -2\eta D_s \mu\Omega/(1-\nu)skT[1-\eta \ln (k_\alpha^2 L_\alpha s)] \tag{28}$$

Integrating eqn (28) from an initial dipole separation, s_0, gives the time to annihilate the dipole:

$$\tau = -\frac{(1-\nu)kT}{4D_s\mu\Omega} s_0^2 \left[\eta_v \ln (k_v^2 L_v s) - \frac{\eta_v}{2} - 1\right] \simeq \frac{s_0}{4v_c} \tag{29}$$

If we consider the mobile dislocation population as a network with all the dislocations taking part in the recovery process, the initial dipole separation is $s_0 = \rho_m^{-1/2}$, and the thermal recovery rate is

$$\dot{\rho}_m = -\frac{2\rho_m}{\tau} = -8\rho_m^{3/2} v_{cm} \tag{30}$$

For the case of the static dislocation population, the initial dipole separation is $s_0 = h$ and the local effective vacancy sink strength is $k_v^2 \simeq 1/h^2$. This gives a thermal recovery rate of

$$\dot{\rho}_s = -\frac{2\rho_s}{\tau} = -8\rho_s \frac{v_{cs}}{h} \tag{31}$$

The possibility that diffusion through the lattice might be short-circuited by dislocation core diffusion must be considered. The process is limited to thermally produced vacancies. This diffusion path has been investigated in some detail by others and used to explain the decrease in creep activation energy and the increase in stress sensitivity for the lower temperature range of creep.[28] The flux of vacancies along the dislocation is

$$j_p = 2\eta_v D_p \sigma_c \Omega/(b + \eta_v L_p)kT \tag{32}$$

where η_v is the transfer coefficient of vacancies from the dislocation core to jogs, which is proportional to the jog concentration. D_p is the core diffusion coefficient, and L_p the path length for diffusion along the core. In this case the jog spacing is likely to be much less than the diffusion path length so eqn (32) reduces to

$$j_p = 2D_p \sigma_c \Omega/L_p kT \tag{33}$$

and the resulting climb velocity is

$$v_c = 2\pi b D_p \sigma_c \Omega/L_p^2 kT \tag{34}$$

The total climb velocity is obtained by summing the components of lattice and pipe diffusion since the two processes can act concurrently. Enhancement of the climb velocity due to pipe diffusion (eqn (34)) can be incorporated in the respective climb velocities of mobile (v_{cm}) and static (v_{cs}) dislocations. Equations (30) and (31) would still be used to compute the climb recovery rates, including the effects of pipe diffusion.

2.5 Dynamic recovery

When dislocation densities become large, it is inevitable that mobile dislocations will occasionally meet dislocations of opposite sign and annihilate. This process is termed dynamic recovery because it is proportional to the strain rate or the dislocation velocity. This process was recognized originally by Johnson and Gilman[33] and by Webster.[34] A simple expression for this type of recovery is

$$\dot{\rho}_m = -\delta(\dot{\rho}_m + \rho_s)\dot{\varepsilon}/b = -\delta\rho_m(\rho_m + \rho_s)v_g \tag{35}$$

where δ is a length parameter related to separation between dislocations for spontaneous annihilation.[3,35] This term in the recovery rate is important because it permits an explanation of the saturation of strain hardening (which leads to the Voce exponential hardening expression[36]), and power-law breakdown for creep at high stresses.[8]

2.6 Stability of subgrains

There are three processes that are known to affect subgrain size during deformation: the subgrain size can coarsen as a result of a reduction of the effective subgrain boundary energy; new subgrains can nucleate from the population of dislocations within the subgrain; and, for high internal stresses, a completely new grain structure can nucleate and sweep through the existing dislocation structure. This last process is termed primary recrystallization and is outside the scope of this paper, although the modelling of dislocation population and the behavior of subgrains could help arrive at a better understanding of the process.

The rate of growth of subgrains may be thought of as the product of a driving pressure and mobility. Let us first look at growth rates in the absence of precipitates. For grain boundary, the driving force for growth is the reduction of grain boundary energy, γ_{gb}. The driving pressure for grain growth is $2\gamma_{gb}/R_{gb}$, where R_{gb} is the grain boundary

radius. For a low-angle subgrain boundary, the energy per unit area is [22]

$$\gamma_{sb} = -\frac{\mu b^2}{4\pi(1-\nu)}\rho_b R_{sb}\ln(bR_{sb}\rho_b) \approx \frac{\mu b^2}{3}\rho_b R_{sb} \tag{36}$$

The energy, E, of one subgrain is simply $4\pi R_{sb}^2\gamma_{sb}$. During subgrain growth, the smallest subgrains collapse their boundaries, coalescing and joining adjacent boundaries. For a collapsing subgrain, the total force acting on the boundary is

$$\frac{dE}{dR_{sb}} = \frac{\partial E}{\partial R_{sb}} + \frac{\partial E}{\partial \rho_b}\frac{d\rho_b}{dR_{sb}} \tag{37}$$

The coalescence of subgrains leads to the annihilation of some of the dislocations. On average, half the dislocations will be lost (i.e. the average dislocation spacing remains constant and $d\rho_b/dR_{sb} = \rho_b/R_{sb}$). The pressure for subgrain growth is

$$p_{sb} = \tfrac{1}{4}\pi R_{sb}^2(dE/dR_{sb}) = \tfrac{4}{3}\mu b^2\rho_b \tag{38}$$

Although it is not possible to describe precisely, the movement of the dislocations in the sub-boundary will be by a combination of glide and climb. The climb process will control the rate. We will assume the following simple forms for core mobility:

$$M_{sb}^c = 2\pi b D_p \Omega/h^2 kT \tag{39}$$

and for lattice diffusion

$$M_{sb}^L = 2\pi\eta_v D_v \Omega/bkT \tag{40}$$

As before, the two mobilities may be summed (i.e. $M_{sb} = M_{sb}^c + M_{sb}^L$).

Two regimes of sub-boundary growth can be identified in the presence of precipitates. If the precipitates are closely spaced, they produce a back pressure opposing sub-boundary motion, a concept first attributed to Zener. The back pressure can be simply estimated from the area of sub-boundary occupied by a precipitate.[21,37] For motion through the precipitates, the pressure of growth must satisfy

$$p_{sb} \geq 2\pi r_p^2 N_p \gamma_{sb} \tag{41}$$

If this is satisfied then the rate of subgrain growth is approximately

$$\partial R_{sb}/\partial t = M_{sb}(p_{sb} - 2\pi r_p^2 N_p \gamma_{sb}) \tag{42}$$

If the inequality (41) is not satisfied, then sub-boundary mobility is controlled by the motion of precipitates. This topic, too specialized for detailed discussion here, has recently been reviewed by Ashby.[37] One example of precipitate motion is by self-diffusion in the matrix and

gives a mobility of

$$M_{sb} = D_s\Omega/4\pi r_p^4 N_p kT \tag{43}$$

The nucleation of new subgrains is less well understood but it is thought to result from the tendency of dislocations for self-organization. Starting with a uniform distribution of screw dislocations, Holt has shown that an instability develops which pulls the dislocation array into a cell-like configuration with a wavelength inversely proportional to the square root of the original dislocation density.[12] Amodeo[13] has performed detailed computer simulations for this self-organization phenomenon. For a population of dislocations with both edge and screw character, the nucleation of subgrains is likely to be dominated by the climb process. We postulate a driving force for nucleation of the form $\mu b(\rho^{1/2} - K_c/2R_{sb})$ where ρ is the sum of the mobile and static dislocations and K_c is the constant from the Holt analysis with a value of around 10.[38,39] The time to nucleate the new subgrain configuration is

$$\tau = (kT/\mu\eta_v K_c \rho^{1/2} D_s)[\rho^{1/2} - (K_c/2R_{sb})]\Omega \tag{44}$$

as the dislocations have to move a distance of around $K_c\rho^{1/2}$ to reach the new configuration. The change in the cell radius is $R - (K_c/2\rho^{1/2})$. Combining these expressions we obtain the rate of subgrain refinement as

$$\partial R_{sb}/\partial t = -\mu\eta_v K_c R_{sb}[(\rho_m + \rho_s)^{1/2} - (K_c/2R_{sb})]\Omega D_s/kT \tag{45}$$

This expression is only applied when $(\rho_s + \rho_m)^{1/2} > K_c/2R_{sb}$.

2.7 The model structure

We now have all the elements that make up the model. In this section, we give a compact description of the rate equations which must be solved simultaneously to obtain the creep strain rate. The glide velocity, climb velocities, and boundary mobility have been described in the previous section; the terms for the subgrain growth rate are subject to the conditions already stated. The only new parameter is ζ which is a measure of the fraction of static dislocations that annihilate when joining the sub-boundary. If ζ were set at 0·5, then all the dislocations would annihilate and the subgrain dislocation density would not grow.

Creep strain—Orowan equation

$$d\varepsilon/dt = b\rho_m v_g \tag{46}$$

Mobile dislocation density

$\partial\rho_m/\partial t$ = Production from the mobile population and subgrain walls—annihilation at subgrain walls—climb recovery—dynamic recovery

$$\frac{\partial\rho_m}{\partial t} = v_g\left[\rho_m^{3/2} + \frac{\beta R_{sb}}{h^2} - \frac{\rho_m}{2R_{sb}} - 8\rho_m^{3/2}\left(\frac{v_{cm}}{v_g}\right) - \delta\rho_m(\rho_m + \rho_s)\right] \quad (47)$$

Static dislocation density

$\partial\rho_s/\partial t$ = Immobilization rate at subgrain walls—climb recovery—dynamic recovery

$$\frac{\partial\rho_s}{\partial t} = v_g\left[\left(\frac{\rho_m}{2R_{sb}}\right) - 8\frac{\rho_s}{h}\left(\frac{v_{cs}}{v_g}\right) - \delta\rho_m\rho_s\right] \quad (48)$$

Boundary dislocation density

$\partial\rho_b/\partial t$ = Production from static population—annihilation by creation of new subgrain surface

$$\frac{d\rho_b}{dt} = 8(1-2\zeta)\rho_s\frac{v_c}{h} - \left(\frac{\rho_b}{R_{sb}}\right)M_{sb}(p_s - 2\pi r_p^2 N_p\gamma_{sb}) \quad (49)$$

Subgrain radius

dR_{sb}/dt = Growth by reduction of surface energy—shrinkage by nucleation

$$\frac{dR_{sb}}{dt} = M_{sb}(p_s - 2\pi r_p^2 N_p\gamma_{sb}) - \mu\eta_v K_c R_{sb}\left[(\rho_m + \rho_s)^{1/2} - \frac{K_c}{2R_{sb}}\right]\frac{\Omega D_s}{kT} \quad (50)$$

3 APPLICATIONS OF THE MODEL TO HT-9

HT-9 is a martensitic steel that is widely used in high temperature applications where resistance to extensive creep deformation is a major concern. Experimental data of creep strains at a number of temperatures and at various levels of applied stress have been obtained from the Sandvik Steel Company[40] and from General Atomics.[41] Amodeo and Ghoniem[42] have previously developed empirical equations for the temperature stress–strain histories of HT-9 when the stress and temperature are both constants. The present model, which is physically based, will be applied to the analysis of the HT-9 data base given in Refs 40–42.

TABLE 1
Table of Parameters

Parameter	*Units*	*Value/Expression*
Glide energy, E_{glide}	eV	2·5
Self energy, E_{self}	eV	2·8
Diffusion coefficient, D_0	cm^2/s	0·2
Burger's vector, b	cm	$2{\cdot}58 \times 10^{-8}$
Atomic volume, Ω	cm^3	$1{\cdot}19 \times 10^{-23}$
Precipitate radius, r_p	Å	405 (at 550 °C)
Precipitate concentration, N_p	cm^{-3}	$1{\cdot}63 \times 10^{10}$ (at 550 °C)
Jog fraction, X_{jog}	—	0·0455
Activation volume, Q	Ω	21·5

A computer program, CREEP, has been developed for the numerical integration of the set of equations (46)–(50). Typical values for HT-9 input parameters are given in Table 1.

Figure 1 is a comparison between the results of the model and available data for 1% creep strain as a function of the applied stress at 600 °C. The effects of an increase in the applied stress on creep strain at a constant temperature are demonstrated in Fig. 2. It is observed that the primary creep transient is reduced by an increase in the applied stress, as is experimentally observed. The secondary creep rate (the slope of the strain–time curve at steady state) increases with the applied stress. This point is further illustrated in Fig. 3 where the secondary creep strain rate is shown as a function of the applied stress. As is characteristic of Class II alloys, the strain rate increases as the fifth power of the applied stress.

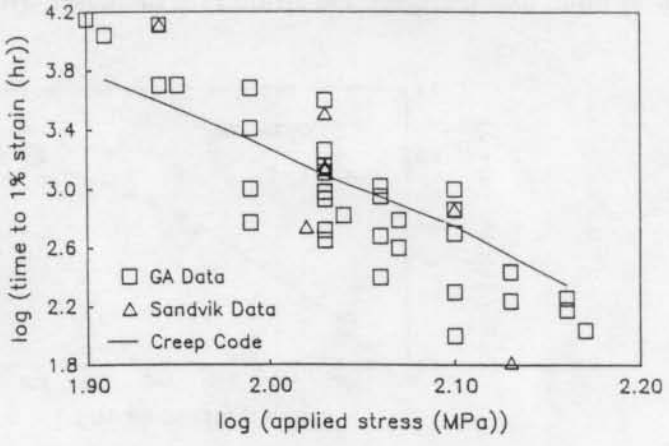

Fig. 1. Time to 1% strain as a function of applied stress for HT-9 at 600 °C.

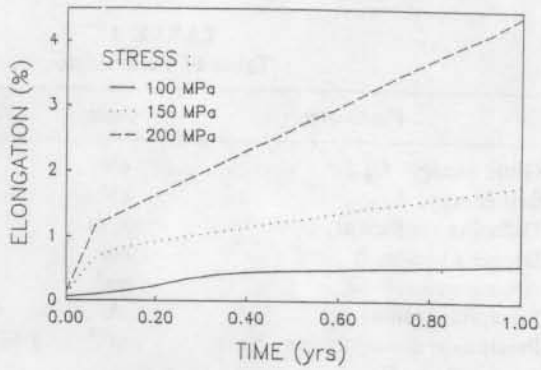

Fig. 2. Creep strain as a function of time at various stress levels for HT-9 at 550 °C.

A small increase in the temperature is known experimentally to accelerate creep deformation. The creep strain as a function of time at various temperatures is shown in Fig. 4. Because of the enhancement of recovery processes at high temperatures, the creep strain dramatically increases with increased temperature. As a consequence of recovery, mobile dislocations can glide easier at high temperatures. The internal stress at steady state is somewhat decreased by an increase in temperature (Fig. 5). The glide velocity of mobile dislocations increases with an increase in temperature, and the net effect is an increase in the creep rate.

Figure 6 shows the time dependence of the strain rate and the components of the Orowan equation at a temperature of 550 °C and an applied stress of 150 MPa. It can be seen that the mobile dislocation density increases gradually with time. The glide velocity also increases with time, and therefore the strain rate increases with time up to about

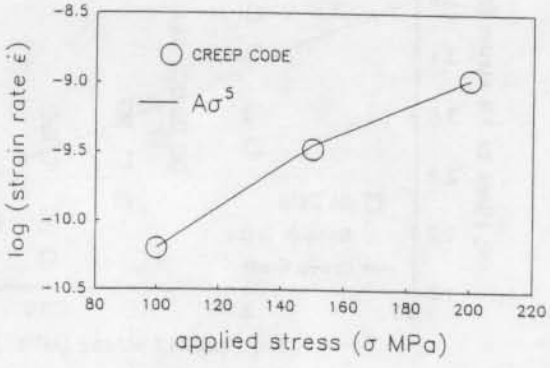

Fig. 3. Strain rate as a function of applied stress for HT-9 at 550 °C.

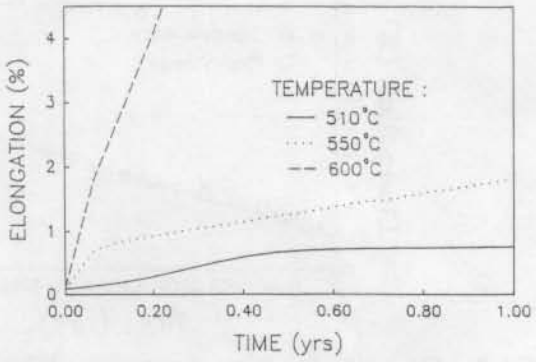

Fig. 4. Creep strain as a function of time at various temperatures for HT-9 at 150 MPa.

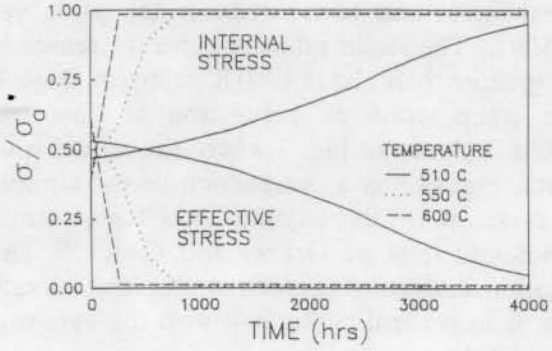

Fig. 5. Evolution of internal and effective stresses for HT-9 at 150 MPa.

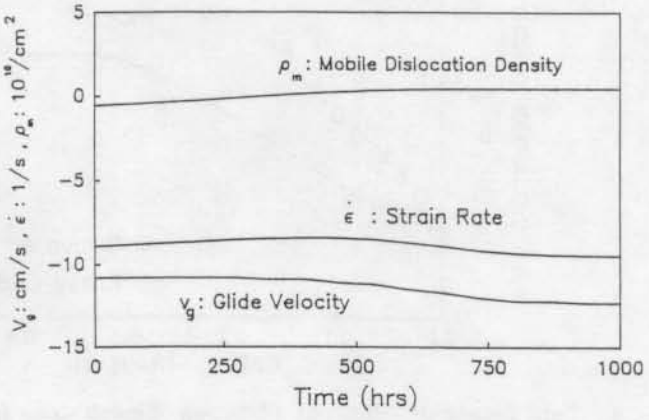

Fig. 6. Evolution of dislocation density, glide velocity, and strain rate for HT-9 at 550 °C and 150 MPa.

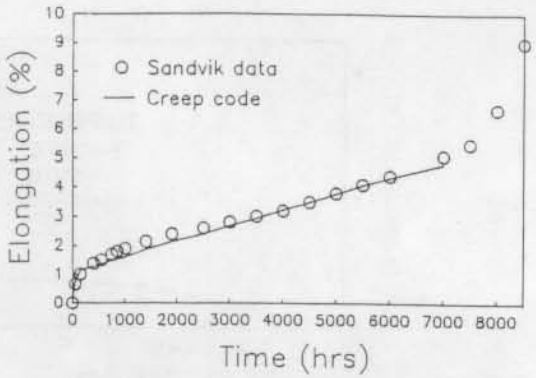

Fig. 7. Elongation as a function of time for HT-9 at 550 °C and 227 MPa.

500 h. The accumulation of the mobile dislocations increases the internal stress and hence reduces the glide velocity for times longer than 500 h. The strain rate therefore decreases to its saturation value at times greater than about 1000 h (compare Figs 4 and 6).

The creep strain as a function of time for HT-9 at 550 °C and 227 MPa is shown in Fig. 7 where the model is compared to experimental data. Figure 8 is a comparison of the computed dislocation density as a function of the accumulated creep strain for α-iron with the experimental data of Orlova and Cadek.[43] The increase in the total dislocation density with creep strain, and its saturation at higher strain values, is in general agreement with the experimental results of Orlova and Cadek.[43]

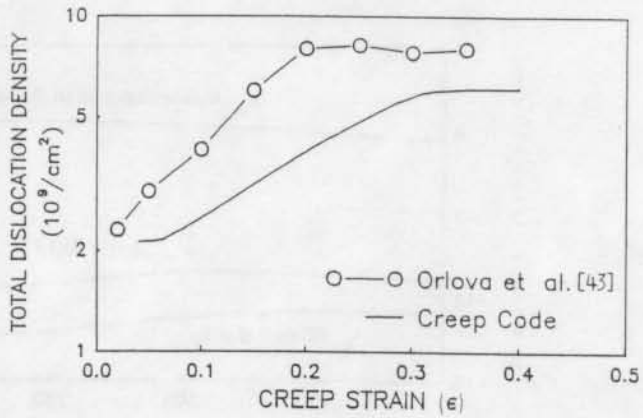

Fig. 8. Total dislocation density as a function of creep strain for α-iron at 600 °C and 73 MPa.

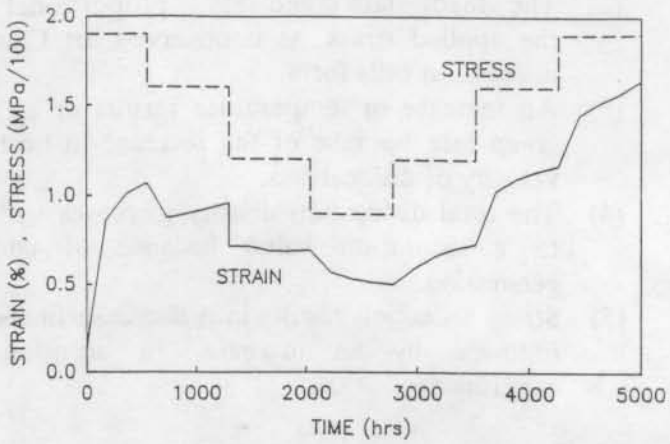

Fig. 9. Time-dependence of accumulated strain for a variable stress history for HT-9 at 550 °C.

To illustrate the utility of our model in representing the creep strain response to a variable stress history, the creep strain is shown as a function of time for HT-9 at 550 °C in Fig. 9. The stress is reduced or increased every 500 h. It is interesting to note that during the first decrease of stress, the strain immediately decreases and then later increases. This behavior is similar to the stress-dip tests which are designed to measure the magnitude of the internal stress. For a short period following the decrease in applied stress, the average effective stress on mobile dislocations becomes negative and the creep strain decreases. Following this behavior, the dislocation density readjusts and the internal stress falls below the current value of the applied stress, leading to an increase in the creep strain.

4 CONCLUSIONS

The present dislocation creep model can be a powerful tool for design of components operating at high temperatures and subjected to a variable history of stress and temperature. The model is based on simple fundamental dislocation rate processes, and is therefore physically based. The adjustable parameters in the model are intended to be flexible enough to represent complex alloys which are often employed in engineering practice. Application of the model to HT-9 gives results which are generally consistent with experimental observations. In particular, the following observations are reproduced by the model:

(1) The primary creep transient decreases with increasing temperature at constant stress.

(2) The steady-state creep rate is proportional to the fifth power of the applied stress, as is observed for Class II alloys in which dislocation cells form.
(3) An increase in temperature results in an enhancement of the creep rate because of the increase in both recovery and glide velocity of dislocations.
(4) The total dislocation density increases with accumulated strain to a saturation value because of continuous dislocation generation.
(5) Stress reduction results in a decrease in the accumulated strain followed by an increase, in accordance with stress-dip experiments.

ACKNOWLEDGEMENTS

This work was supported by the US Department of Energy, Office of Fusion Energy, Grant No. DE-FG03-84ER52110, with UCLA. The authors would also like to acknowledge the support provided by the Theoretical Physics Division, UK Atomic Energy Authority, Harwell, UK.

REFERENCES

1. Bullough, R., Dislocations and radiation damage, *Proc. Conf. on Dislocations and the Properties of Real Materials,* Royal Society of London, 1984 (Institute of Metals), p. 283.
2. Nabarro, F. R. N., *Phil. Mag.,* **16** (1967) 231.
3. Bullough, R., Finnis, M. W. & Wood, M. H., *J. Nucl. Mater.,* **103 & 104** (1981) 1263.
4. Bullough, R., Finnis, M. W., Matthews, J. R. & Wood, M. H., Progress in the theory of radiation and thermal creep, *Proc. Conf. on Dimensional Stability of Irradiated Metals and Alloys,* BNES, Brighton. 1983, paper 22, vol. 1, p. 25.
5. Heald, P. T. & Speight, M. V., *Phil. Mag.,* **29** (1974) 1075.
6. Bullough, R. & Willis, J. R., *Phil. Mag.,* **31** (1975) 855.
7. Nabarro, F. R. N., Bullough, R. & Matthews, J. R., *Acta Metall.,* **30** (1982) 1761.
8. Gittus, J. H., *Phil. Mag.,* **25**(5) (1972) 1233.
9. Gittus, J. H., *Phil. Mag.,* **34** (1977) 401.
10. Matthews, J. R., *A Simple Dislocation Model for High Temperature Deformation,* AERE-R. 11564, Harwell Lab. Rep., 1985.
11. Amodeo, R. J. & Ghoniem, N. M., *Res Mechanica,* **23** (1988) 137.
12. Holt, D., *J. Appl. Phys.,* **41** (1970) 3197.

13. Amodeo, R. J., *Dynamic Simulation of Dislocation Pattern Formation in Metals during High Temperature Monotonic and Cyclic Deformation,* PhD thesis, University of California at Los Angeles, Los Angeles, CA, 1988.
14. Takeuchi, S. & Argon, A. S., *J. Mater. Sci.*, **11** (1976) 1542.
15. Langdon, T. G., Dislocations and creep, *Proc. Conf. on Dislocations and the Properties of Real Materials,* Royal Society of London, 1984 (Institute of Metals), p. 221.
16. Challenger, K. D. & Moteff, J., *Metall. Trans.*, **4** (1973) 749.
17. Michel, D. J., Moteff, J. & Lovell, A. J., *Acta Metall.*, **21** (1973) 1269.
18. Cuddy, L. J., *Metall. Trans.*, **1** (1970) 395.
19. Li, J. C. M., *J. Appl. Phys.*, **33** (1962) 2958.
20. Sandström, R., *Acta Metall.*, **25** (1977) 897.
21. Sandström, R., *Acta Metall.*, **25** (1977) 905.
22. Friedel, J., *Dislocations,* Pergamon Press, Oxford, 1964.
23. Nabarro, F. R. N., Solution hardening, *Proc. Conf. on Dislocations and the Properties of Real Materials,* Royal Society of London, 1984 (Institute of Metals), p. 152.
24. Takeuchi, S. & Argon, A. S., *Acta Metall.*, **24** (1976) 883.
25. Cottrell, A. H., *Prog. Metall. Physics,* **1** (1952) 77.
26. Hirth, J. P. & Lothe, J., *Theory of Dislocations,* McGraw-Hill, New York, 1968, Chapter 16.
27. Rauh, H. & Bullough, R., *Phil. Mag.*, **52** (1985) 33.
28. Evans, H. E. & Knowles, G., *Acta Metall.*, **25** (1977) 963.
29. Brailsford, A. D. & Bullough, R., *Phil. Trans. Soc. London,* **302** (1981) 87.
30. Quigley, T. M., *Theory of Radiation Damage in Fusion Materials,* AERE-TP. 954, Harwell Lab. Rep., 1982.
31. Argon, A. S. & Moffatt, W. C., *Acta Metall.*, **29** (1981) 293.
32. Mohamed, F. A. & Langdon, T. G., *Acta Metall.*, **22** (1974) 779.
33. Johnson, W. G. & Gilman, J. J., *J. Appl. Phys.*, **30** (1950) 129.
34. Webster, G. A., *Phil. Mag.*, **14** (1966) 775.
35. Essmann, N. & Muhgrabi, H., *Phil. Mag.*, **40** (1979) 731.
36. Voce, E., *J. Inst. Metals,* **74** (1948) 537.
37. Ashby, M. F., The influence of particles on boundary mobility, *Proc. 1st Risø Int. Symp. on Metallurgy and Materials Science Recrystallisation and Grain Growth of Multi-Phase and Particle Containing Materials.* Risø National Laboratory, Denmark, 1980.
38. Gittus, J. H., *Phil. Mag.*, **35**(2) (1977) 293.
39. Gittus, J. H., *Phil. Mag.*, **39**(6) (1979) 829.
40. Amodeo, R. J. & Ghoniem, N. M., *Constitutive design equations for creep deformation of HT-9,* PPG-743, University of California Los Angeles report, 1983.
41. Wattier, J. G., in *Materials Handbook for Fusion Energy Systems,* DOE/TIC-10122, File Codes AA01-2202/-2206, McDonnell–Douglas Astronautics Co., St Louis, Missouri, 1985.
42. Amodeo, R. J. & Ghoniem, N. M., *J. Nucl. Mater.*, **122**(1–3) (1984) 91.
43. Orlova, A. & Cadek, J., *Mater. Sci. Eng.*, **77** (1986) 1.